Published in final edited form as:
Ann Neurol. 2012 January ; 71(1): 93–109. doi:10.1002/ana.22627.

ARRESTED PRE-OLIGODENDROCYTE MATURATION CONTRIBUTES TO MYELINATION FAILURE IN PREMATURE INFANTS

Joshua R. Buser, B.S.[1], **Jennifer Maire, B.S.**[1], **Art Riddle, Ph.D.**[1], **Xi Gong, M.D.**[1], **Thuan Nguyen, Ph.D.**[3], **Kerst Nelson, B.A.**[1], **Ning Ling Luo, M.D.**[1], **Jennifer Ren**[1], **Jaime Struve, B.S.**[5], **Larry S. Sherman, Ph.D**[5], **Steven P. Miller, MDCM**[6], **Vann Chau, M.D.**[6], **Glenda Hendson, M.D.**[7], **Praveen Ballabh, M.D.**[8], **Marjorie R. Grafe, M.D.Ph.D.**[4], and **Stephen A. Back, M.D.Ph.D.**[1,2]

[1]Department of Pediatrics, Oregon Health & Science University, Portland, OR

[2]Department of Neurology, Oregon Health & Science University, Portland, OR

[3]Department of Public Health and Preventive Medicine, Oregon Health & Science University, Portland, OR

[4]Department of Pathology, Oregon Health & Science University, Portland, OR

[5]Division of Neuroscience, Oregon National Primate Research Center, Hillsboro, OR

[6]Department of Pediatrics, University of British Columbia, Vancouver, B.C., Canada

[7]Department of Pathology, University of British Columbia, Vancouver, B.C., Canada

[8]Departments of Pediatrics and Anatomy & Cell Biology, New York Medical College, Valhalla, New York

Abstract

Objective—The major form of MRI-defined white matter injury (WMI) comprises diffuse lesions where the burden of small necrotic foci (microscopic necrosis) is poorly defined. We hypothesized that myelination failure associated with diffuse WMI involves an aberrant injury response linked to arrested pre-oligodendrocyte (preOL) maturation in reactive astrocyte-rich lesions.

Methods—A retrospective autopsy series (1983–2000) was selected for cases with diffuse WMI and analyzed relative to prospectively-collected contemporary cases (2003–2010). Controls were age and region-matched to address regional variation in preOL maturation. Successive oligodendrocyte stages were analyzed with lineage-specific markers. Microscopic necrosis was quantified with microglial markers. Axon injury markers defined the burden of axonopathy. Extracellular matrix remodelling was defined by detection of hyaluronic acid (HA), an inhibitor of preOL maturation, and the HA receptor, CD44.

Results—In the contemporary case series, diffuse WMI was accompanied by a significant reduction in the burden of microscopic necrosis and axonopathy. Diffuse astrogliosis extended into the lesion surround with elevated HA and astrocyte-expressed CD44. The total population of OL lineage stages was significantly increased in lesions. This increase coincided with significant expansion of the preOL pool.

Correspondence to: Stephen A. Back, M.D., Ph.D., Department of Pediatrics, Mail Code L481, Oregon Health & Science University, 3181 SW Sam Jackson Park Road, Portland, Oregon 97239-3098, Phone: 503-494-0906; Fax: 503-494-0428; Backs@ohsu.edu.

Interpretation—Although these data confirm that microscopic necrosis occurs in contemporary cases, the markedly decreased burden supports that it does not contribute substantially to myelination failure. The primary mechanism of myelination failure involves a disrupted cellular response whereby preOLs fail to differentiate in diffuse astrogliotic lesions. Pre-oligodendrocyte maturation arrest converts chronic WMI to a more immature state related to the burden of astrogliosis.

Cerebral palsy (CP) is a major cause of chronic neurological morbidity and mortality in children.[1] In a large population based study of children with CP, perinatal white matter injury (WMI), including periventricular leukomalacia (PVL), was the most common finding, seen in almost half of affected children (42·5%).[2] Since the underlying brain injury mostly arises from destructive processes, development of therapies for CP has been hampered by the prevailing notion that there is limited potential for recovery.

The propensity for myelination failure in chronic WMI is the central pathological feature that distinguishes brain injury in the preterm survivor from other forms of CP that principally involve gray matter. A recent study proposed three potential mechanism for myelination failure related to WMI, but did not analyze the role of OL progenitors.[3] Hence, controversy exists regarding the mechanism of myelination failure and whether it involves axonopathy, arrested OL lineage progression or disturbances in myelination initiated by OLs.

With advances in neonatal intensive care and neuro-imaging, there has been a pronounced shift in the features of WMI as defined by quantitative and diffusion-weighted MRI.[4–6] Whereas PVL was previously the major form of brain injury in pre-term survivors, the incidence of large necrotic lesions has markedly declined.[7] Recent MRI studies have defined a milder form of WMI characterized by focal or diffuse non-destructive lesions.[8] However, recent neuropathology studies found a 34% incidence of microscopic necrosis that is poorly defined by MRI and involves axonopathy.[9, 10] Since the burden of microscopic necrosis in WMI has not been defined, the contribution of axonopathy to myelination failure is unclear.

Pre-oligodendrocytes (pre-OL) generate the mature OLs required for CNS myelination,[11] and predominate throughout a critical developmental window that coincides with the high-risk period for WMI.[12] Since preOLs selectively degenerate in acute WMI,[13, 14] myelination failure was proposed to arise from a persistent deficit of pre-OLs.[11] However, two related sets of observations challenged this hypothesis and lead us to test whether myelination failure involves an aberrant injury response linked to arrested pre-OL maturation. First, in adult WMI, reactive astrocyte-derived hyaluronic acid accumulates in the glial scar and reversibly inhibits preOL differentiation and myelination.[15] Secondly, despite substantial preOL degeneration in response to hypoxia-ischemia in preterm-equivalent rodents, surviving preOLs rapidly increase in number to repopulate lesions.[16]

Here we demonstrate that burden of necrosis and accompanying axonopathy was markedly decreased in contemporary WMI, which questions the notion that myelination failure primarily arises from small foci of necrosis not detected by MRI.[11] Rather, human WMI has the potential for regeneration and repair through injury response mechanisms intrinsic to oligodendrocyte (OL) progenitors that regenerate preOLs lost during acute WMI.[13, 14] However, myelination failure arises from failure of preOLs to generate oligodendrocytes.

Methods

Study Populations and Histopathological Criteria for Case Selection

We studied two cohorts of autopsy brains to define mechanisms of myelination failure associated with diffuse WMI (Fig. 1). Cohort 1 (1983–2000) comprised retrospectively collected archival cases (formalin-fixed and paraffin-embedded) to analyze total OL lineage cells in chronic WMI. Since diffuse lesions without overt necrosis are presently the major form of MRI-defined WMI,[8] cohort 1 cases were selected on initial review of hematoxylin and eosin (H & E) stained sections that had diffuse astrogliosis as the predominant form of WMI. A prospective series (2003–2010) comprised WMI cases representative of the population of infants managed in the contemporary intensive care setting. Autopsy brains were fixed in paraformaldehyde. Human pre-myelinating OL lineage stages are optimally visualized in paraformaldehyde-fixed tissue and were not detectable in formalin-fixed paraffin-embedded tissue (cohort 1).[12]

Several strategies were taken to provide comparable analysis of cohorts 1 and 2 (Fig. 1). In both cohorts, cases were selected with the same histopathological and exclusion criteria. A combination of H & E and GFAP staining was analyzed to confirm that both cohorts had a similar magnitude of white matter astrogliosis. A similar extent of microscopic necrosis was determined by analysis of activated microglia and macrophages and confirmed with markers of axonopathy. Since the density of OL lineage cells varies markedly between regions,[13] we age and region-matched our cases, in contrast to prior studies that did not region-match prior to quantification of OL lineage cells pooled from multiple cerebral regions.[3]

Features of Cohort 1 (Table 1)

After full IRB review and approval, a retrospective review of pediatric autopsy cases from Children's and Women's Hospital, University of British Columbia identified 27 cases with chronic WMI collected from 1983–2000. Paraffin-embedded tissue sections from multiple brain regions for each case were stained with H & E and reviewed by MRG and SAB. From this case review, 17 cases were identified that met one or more of the following histopathological criteria for a diagnosis of chronic WMI: 1) focal hypertrophic reactive astrocytosis within the subventricular zone (SVZ); 2) focal or diffuse hypertrophic reactive astrocytosis within deep cerebral white matter; 3) presence of scattered but not large aggregates of hypertrophied transforming microglia. Two cases with intrauterine fetal death were excluded. Eight cases were excluded where the predominant lesion was significant necrotic WMI (PVL): 1) acute (coagulative necrosis) or cavitary necrosis in the SVZ or white matter with focal collections of phagocytic/lipid-laden macrophages or reactive hypertrophied vascular endothelium; 2) mineralization of cells in the gray or white matter; 3) features of intraventricular hemorrhage with parenchymal extension with or without hemosiderin-laden macrophages; 4) microscopic or macroscopic features of hemorrhagic infarction; 5) cerebral cortical ischemic changes such as focal neuronal necrosis or pan-laminar necrosis. Ten blocks from 7 controls were age and region-matched to one or more of 14 of the 17 chronic WMI cases. H & E stained sections from controls were reviewed by MRG and identified from the pediatric autopsy population of OHSU.[13] Within the tissue blocks studied, controls lacked cerebral gray or white matter injury. Three cases which lacked a stringent age and region-matched control were only included in cohort analysis. Postmortem interval, race, and sex did not different significantly between control and WMI cases (Table 1).

Features of Cohort 2 (Table 2)

Fifteen brains were prospectively collected at autopsy (2003–2009) at the Maria Ferreri Children's Hospital, Westchester Medical Center, Valhalla, New York and at OHSU (2003–

2010). Tissue blocks, which contained frontal periventricular white matter at the level of the anterior horn of the lateral ventricle, were fixed for 24 h by immersion in ice-cold 4% paraformaldehyde in 0·1M phosphate buffer, pH 7·4 followed by cryoprotection in 20% sucrose.[17] Tissue was frozen in isopentane:dry ice, embedded in OCT, and sectioned on a cryostat at 12 μm. Cases were analyzed without knowledge of the neuropathological diagnosis or clinical history. Assignment to the control or WMI group was made at the conclusion of the analysis by post-hoc H & E review and quantification of astrocytes (below). All lesions had minimal or no necrosis, which minimized the potential for variable tissue shrinkage. The same histopathological criteria for chronic WMI and the same exclusion criteria were applied as for the cases in Table 1. Three cases were excluded due to gestational age outside of the range under study and two were too fragile to generate sufficient frozen tissue sections.

Quantification of Astrocytes by Cavalieri Point Counting

Paraffin-embedded tissue sections (6 μm) were stained by fluorescence immunohistochemistry with rabbit anti-bovine glial fibrillary acidic protein (GFAP) antisera (1:1000; Z-0334; DAKO, Carpinteria, CA) and nuclei visualized by counterstain with Hoechst 33342.[16] We employed a method based on Cavalieri point counting to estimate the area fraction of GFAP-labeled somata in chronic WMI lesions relative to controls.[18] The method was validated against analysis of H&E-stained tissue sections that were first digitized with a Nikon Cool Scan IV color slide scanner to obtain a low power image of the entire section. The approximate boundaries of lesions were defined on each digitized image with the line tool in Adobe Photoshop. For each H & E-stained section, the boundaries of a near adjacent GFAP-stained section were traced in Stereo Investigator (Microbrightfield, Williston, VT), with a motorized x, y stage on a Leica DMIRE2 inverted fluorescent microscope. With NIH ImageJ, the digitized image of the H & E-stained section was visually aligned to the outline of the GFAP-stained section, and the ROI transferred to the traced GFAP outline. Images at 40× magnification were captured from points on randomly placed and oriented grids within the ROI and in white matter outside of the boundaries of the ROI (at least 24 images for each).

To estimate the magnitude of astroglial activation, a systematic, unbiased estimate of GFAP-stained cell body area was made with the Cavalieri point-counting method.[18] Each 40× image (88,700 μm^2) was opened with ImageJ, and a 50 μm^2 randomly oriented and positioned grid was overlayed onto the image. The grid points that fell onto a GFAP positive cell body were counted by a blinded observer. Only the astrocyte cell body was included in the count and processes were excluded. The transition between cell body and process was visually delineated, where the width of the process was ~1/3 the diameter of the largest circle that could be inscribed within the cell body.

Quantification of CD44-labeled Cells and Hyaluronan (HA) Detection

Tissue was double-labeled by fluorescence immunohistochemistry for GFAP and CD44 with mouse anti-human CD44 antibody (Hermes-3, ATCC, Manassas, Virginia).[15] CD44 expression in human microglia was evaluated by double-labeling for CD44 and biotinylated tomato lectin (1:100; B-1175; Vector Laboratories, Burlingame, CA). Five tissue blocks from four controls were age and region-matched to 6 blocks from six chronic WMI cases that ranged in post-conceptional age from 32–38 weeks. The density of CD44-labeled cells was determined in a total of 528 fields also analyzed for GFAP area fraction, above. In WMI cases, the regions sampled included both lesion ROIs (n=24) and adjacent peri-lesion areas (n=24). Corresponding ROIs were analyzed for control (n=20) and peri-control (n=20). To visualize HA, a biotinylated hyaluronan binding protein (HABP; 1:200; Seikagaku, Japan)[15]

was detected with Rhodamine Red X-conjugated Streptavidin (1:400; 016-290-084; Jackson ImmunoResearch, West Grove, PA).

Quantification of Iba1-labeled microglia

Tissue sections from the cases stained for GFAP, above, were also stained for Iba1, which labels all human microglia and macrophages.[19] After antigen retrieval (10 min at 95°C in 10 mM sodium citrate buffer, pH 6·0), tissue was incubated at 2–4°C for 3 days with a rabbit polyclonal antiserum (019-18741; 1:500 in PBS with 0·1% triton X-100; Wako Chemicals, Richmond, VA) raised against Iba1. Primary antiserum was visualized with a goat anti-rabbit biotinylated antibody (1:200, 111-065-046; Jackson ImmunoResearch) and a peroxidase-immunoperoxidase staining protocol with nickel silver enhancement (SK-4100; Vector Laboratories). Iba1 staining was analyzed in an unbiased fashion as adapted from previously described methods.[20] Briefly, the entire lesion or control ROI, as described for GFAP above, was analyzed. A pixel-intensity histogram was generated using ImageJ and exported to a spreadsheet. The peak of the histogram was calculated using the three highest frequency bins. The histogram curve was integrated from this peak towards the background pixel side of the histogram and a value obtained for the area of this region. This area was then doubled to estimate the entire histogram and the total distribution of background pixels in the image. The total background area was subtracted from the total area of the pixel-intensity histogram to define the Iba1-labeled area.

Analysis of Necrotic WMI

Regions of necrosis (microcysts) were identified on H & E stained sections and analyzed in near-adjacent sections where focal collections of activated-appearing microglia and macrophages coincided with necrotic foci. The mean cross-sectional diameter of necrotic foci was defined as the average of the maximum and minimum diameters of microcysts estimated by an elliptical area. For cohort 1, the percentage area comprised by microcysts in a given lesion was estimated in ImageJ by measuring the area bounded by the lesion and the microcyt. Lesion boundaries were defined in H & E stained sections and aligned with the corresponding Iba1 stained tissue section using ImageJ. For cohort 2, microglial and macrophages were visualized with tomato lectin, as described above, rather than Iba1, to optimize tissue integrity for frozen sections.

Analysis of Axonopathy

Degenerating axons were visualized in archival cases (Table 1) by immunohistochemical detection of beta-amyloid precursor protein (βAPP; MAB348, 1:4000; Millipore, Billerica, MA) and caspase-cleaved actin with the fractin antibody.[10, 21] Axon integrity in cohort 2 cases was detected with the anti-neurofilament antibody, SMI-312 (1:1000; Covance, Emeryville, CA), visualized as described for paraformaldehyde-fixed tissue.[22] To distinguish the morphology of axons in necrotic foci, tissue sections were double-labeled for SMI-312 and tomato lectin to visualize microglia and macrophages.

Quantification of Olig2-labeled cells

After antigen retrieval (10 min at 95°C in 10 mM sodium citrate buffer, pH 6·0), tissue was incubated with a rabbit polyclonal antiserum (1:10,000 in PBS with 0·1% triton X-100) raised against the nuclear transcription factor Olig2 (generous gift of Dr. John Alberta, Dana Farber Cancer Institute, Boston) that labels all cells of the OL lineage.[20] Primary antiserum was visualized with a goat anti-rabbit biotinylated antibody (1:200, 111-065-046; Jackson ImmunoResearch) and a peroxidase-immunoperoxidase staining protocol with nickel silver enhancement (SK-4100; Vector Laboratories). Density of Olig2-labeled nuclei was determined by investigators blinded to pathological diagnosis from a minimum of ten

digitized bright-field images (40×) randomly acquired in at least three near-adjacent sections with a Leica DMRA upright microscope coupled to a Leica DFC-290 digital color camera. Myelination was assessed by staining for myelin basic protein (MBP) with SMI-99P (1:1000; Covance, Emeryville, CA).

Quantification of pre-myelinating stages of the oligodendrocyte lineage

In preterm human brains, the O1 antibody labels immature OLs and the O4 antibody labels the total pool of late OL progenitors (preOLs; O4+O1−) and immature OLs (O4+O1+)[12]. Six adjacent tissue sections were alternately stained for GFAP/O4 or GFAP/O1 by fluorescence immunohistochemistry.[16] Tissue sections were counterstained with Hoechst to define boundaries between the deep white matter and SVZ. ROIs in deep white matter were selected without reference to the GFAP, O4 or O1 staining. Within each ROI, fifteen fields were counted in each of three sections for counts of O4, O1 and GFAP area fraction. Cell profiles that contained a nucleus, visualized with Hoechst, were counted with a 40× objective equipped with a counting grid (0·0625 mm^2/field), and the relative percentages and density of preOLs and immature OLs calculated.[12] Degenerating cells were confirmed to contain a pyknotic nucleus.

Analysis of Cell Proliferation and Cell death in Chronic Lesions

Cell proliferation was determined by immunohistochemical detection of Ki67 (pre-diluted, clone 30-9; 790–4286; Ventana Medical Systems, Tuscon, AZ). Cleaved caspase-3 (1:1000; #9664; Cell Signaling Technologies, Danvers, MA) was visualized as previously described.[16]

Statistical Analysis

Data analysis was performed using SAS software 9·2 (SAS Institute Inc., Cary, NC, USA.) Box and whisker plots represent the 25^{th} and 75^{th} percentiles, median (central line) and mean (central box). Confidence intervals represent the differences between groups. The necessary assumptions (e.g., normality, equal variance) were tested before the following analyses were performed. Supplemental Table 1 includes 21 sub-tables that provide a summary of all statistical analyses performed. All group analyses were tested for independent effects of post-conceptional age, survival time, sex, and post-mortem interval. If any confounding effects were found, the adjusted value was reported. Analysis of GFAP area fraction and Olig2 density for each WMI case relative to a matched control was performed using a repeated measure ANOVA (rmANOVA). To analyze the association between CD44 and GFAP we employed a mixed effects model (MEM) with two-level nested error regression. The MEM was also applied for analysis of Olig2, GFAP, and CD44 across the entire cohort. Two-level nested error regression was applied, because, within a case, each lesion or corresponding control region was analyzed for multiple ROIs (level 2) and multiple high power fields were analyzed within each ROI (level 1) (See Supplemental Table 1). The following studies tested for an association across the entire cohort using a general linear model (GLM): Iba1 area fraction vs. GFAP area fraction; Olig2 density vs. GFAP area fraction; and preOL density vs. GFAP area fraction. Differences in Iba1 area fraction, preOL density, immature OL density, and percentage of immature OLs were also examined using a GLM. Reported p-values were corrected for multiple comparisons by the Bonferroni method. All statistical tests were considered significant at a p=0·05 level of error.

Results

Unbiased quantification of white matter astrogliosis identified diffuse graded astroglial reaction in chronic WMI

Although diffuse reactive astrocyte response is the most commonly observed feature of chronic WMI, seen in greater than 80% of cases,[9] there is no consensus on the optimal approach to distinguish reactive astrocytes from resting ones or oligodendrocyte progenitors ("myelination glia").[23, 24] Prior studies relied on non-quantitative approaches to define astrogliosis in WMI.[3, 9, 25] We first quantified astrogliosis in both cohorts with the Cavalieri point counting method,[18] which generated an area-fraction for GFAP-labeled astrocytes in controls (Fig. 2A; Supplemental Fig. 1A) and WMI cases (Fig. 2B; Supplemental Fig. 1B). The approach for GFAP quantification is shown in Fig. 2C where lesions and region-matched controls were initially defined by review of H & E stained sections. The GFAP area fraction was significantly elevated in lesions relative to controls in both the retrospective (Fig. 2D; 95% CI 0.019—0.022; p<0·0001, Supplemental Table S·1) and prospective (Suppl. Fig. 1C; 0.0025—0.0080; p=0·0012, Table S·14) cohorts. To determine the number of WMI cases with elevated astrogliosis, we identified controls that were both age and region-matched to individual WMI cases. In 12 out of 14 WMI cases from the retrospective cohort, GFAP was significantly elevated relative to controls (p<0·007, Table S·20). Hence, diffuse astrogliosis was present in 86% of these cases, consistent with prior findings.[9]

We next determined whether astroglial activation differs in lesions and adjacent peri-lesions relative to control and peri-control regions (Fig. 2C). We analyzed the retrospective cohort where tissue preservation was optimal to define the boundaries of large lesions relative to routine histology (see Methods). When analyzed for the entire cohort, GFAP in the peri-lesions differed significantly from both corresponding peri-control regions (Fig. 2D; 0.011—0.014; p<0·0001, Table S·1) and lesions (0.007—0.0098; p<0·0001). In 8 of 14 cases, GFAP was significantly increased in the peri-lesion relative to peri-control white matter (p<0·02, Table S·20). Moreover, within WMI cases the peri-lesion was signicantly lower than the lesion in 9 out of 17 cases (p<0·03, Table S·20). The elevated but intermediate GFAP levels in the peri-lesions, thus, support that chronic WMI is characterized by an astroglial reaction that is more extensive than feasible to define by standard histopathological review. Hence, astrocytes appeared to be diffusely activated both within lesions and the peri-lesion surround.

The transmembrane HA receptor CD44 is an independent marker of astrogliosis in hyaluronan (HA)-enriched lesions

In adult CNS white matter HA accumulates in areas of WM damage and demyelination and blocks preOL maturation.[15, 26] The HA receptor CD44 is up-regulated under conditions of free radical injury, including ischemia.[27] To determine whether HA and CD44 are also abnormally expressed in WMI, we first defined the cell types that express CD44 in chronic lesions. Double-labeling for CD44 (Fig. 3A; red) and GFAP (Fig. 3B; green) showed that CD44 and GFAP were co-localized in most astrocytes (Fig. 3C). CD44 had a more diffuse cellular distribution than GFAP, reflecting its role as a transmembrane glycoprotein receptor.[26] CD44 (Fig. 3D; green) was not detected in microglia, macrophages (Fig. 3D; red) or pre-myelinating OL lineage cells stained with the O4 antibody (Fig. 3E; green).

Since CD44 was highly expressed on astrocytes, we determined if CD44 might be an independent marker of chronic WMI. Figure 3F shows that GFAP and CD44 levels were significantly associated (p<0·0001, Table S·2). Control cases (green) had a significantly lower density of CD44 relative to lesions (red) (3·5—13; p<0·005, Table S·3), whereas the peri-lesions (blue) were intermediate in density between control (−0·2—9·1; p=0·06) and

lesion ROIs (−0·02—7·4; p=0·05). Thus, CD44 was a robust independent marker of WMI that, like GFAP, identified diffuse astrocyte activation within chronic lesions and the peri-lesion surround.

Double-labeling for CD44 and a hyaluronan binding protein demonstrated that elevated HA staining (Fig. 3G; red) was diffusely distributed in the extracellular matrix in regions enriched in $CD44^+$ reactive astrocytes (Fig. 3G; green). The intensity of HA staining was low in regions with a paucity of GFAP-labeled astrocytes (Fig. 3H) whereas, elevated pericellular HA staining was closely associated with reactive astrocytes (Fig. 3I). This finding is consistent with rodent and human demyelinating lesions where HA accumulates coincident with elevated CD44 expression.[15]

Microgliosis is associated with astrogliosis as an independent marker of chronic WMI

Microglial activation occurs during normal human white matter development and neuro-inflammatory events related to the pathogenesis of early PVL.[28, 29] To determine if microglial activation also occurs in chronic WMI, we quantified the microglial marker Iba1 in the retrospective cohort. Control white matter typically contained numerous resting or non-ramified microglia (Fig. 4A). In contrast, microglia in chronic lesions often displayed a reactive hypertrophic morphology consistent with microglial activation (Fig. 4B). We quantified Iba1 labeled microglia in the same ROIs analyzed for GFAP (Fig. 2) and found a significant elevation in Iba1-labeled microglia in WMI cases relative to controls (Fig. 4C; 0·03—0·20; p=0·01, Table S·4). The magnitude of Iba1 staining was significantly associated with the level of GFAP (Fig. 4D; p=0·002, Table S·5) as a third independent marker of chronic WMI. Hence, microglial activation not only occurs in early WMI but appears to persist in chronic lesions with diffuse astrogliosis.

The burden of necrotic WMI was markedly reduced in contemporary cases

To estimate the relative burden of injury contributed by white matter necrosis in the two cohorts, we identified necrotic foci on H & E stained sections that typically were in deep periventricular white matter below the diffuse WMI. In adjacent sections, we determined the total area that contained focal collections of activated microglial and macrophages in the white matter. The mean total area of necrosis was significantly higher (0·10—3·29; p=0·006, Table S·16) in the retrospective cohort (2·3 ± 2·9 mm^2) relative to the contemporary cohort (0·2 ± 0·5 mm^2). The incidence of necrotic WMI was also significantly lower for the contemporary cohort (p=0·02; Table S·18). Hence, the total burden and incidence of necrosis was significantly lower in contemporary cases, supporting that the severity of WMI is declining.

We next determined the incidence and burden of microscopic necrosis (microcysts), previously defined as focal lesions with a diameter of ~1 mm (Fig. 4E).[3, 9] Consistent with these prior studies, microcysts in the retrospective cohort had a similar (p=0·15, Table S·15) mean diameter of 0·8 ± 0·5 mm vs 0·4 ± 0·5 in the contemporary cohort, where only microcysts were identified. Microcysts were identified in none of the controls but were present in 59% of retrospective cases vs. 36% of contemporary cases (p=0·44, Table S·19). The mean total area of microcysts was low in both the retrospective (0·4 ± 0·6 mm^2) and contemporary cohorts (0·2 ± 0·5 mm^2) (p=0·15, Table S·17). The low overall burden of microscopic necrosis was confirmed in the more severely injured retrospective cohort where microcysts comprised 2·5 ± 2·2% of the total lesion area identified with diffuse astrogliosis.

Axonopathy is a minor contributor to myelination failure

Diffuse axonal injury is associated with large necrotic lesions in infants with PVL.[10] We determined the extent of axonal injury associated with microcysts. In both cohorts,

axonopathy typically coincided with microcysts. Axonopathy within microcysts was observed in retrospective cases with the fractin antibody that labels caspase-cleaved actin (Fig. 4F).[10] Dilated and dystrophic axons were abundantly visualized at the periphery of microcysts, but were uncommon in the necrotic core. Staining for β-amyloid precursor protein (βAPP), an additional marker of axonopathy,[10, 30] demonstrated that βAPP accumulated throughout microscopic foci of necrosis (Supplemental Fig. 2) The βAPP was mostly restricted to the microcysts, but was more diffusely seen in the adjacent reactive astrogliosis in two cases where larger necrotic foci occurred.[10] In contemporary cases, degenerating axons were only detected in microcysts, as determined by double staining for Iba1 and the neurofilament protein antibody, SMI-312 (Supplemental Fig. 3). Hence, in contemporary cases, the major form of pathology associated with chronic WMI was diffuse reactive astrogliosis, whereas microscopic necrosis with axonopathy was a minor component.

OL Lineage cells are enriched rather than depleted in chronic WMI

Since the burden of axonopathy was low in contemporary cases, we addressed an alternative hypothesis that myelination failure in WMI is related to changes in density of the total population of oligodendrocyte (OL) lineage cells available for myelination. Since preOLs selectively degenerate in acute WMI,[13, 14] we predicted that the density of Olig2-labeled cells would decrease in chronic lesions. We first quantified the density of total OL lineage cells with the pan-OL marker/transcription factor Olig2 (Fig. 5A, B) in the same ROIs where astrogliosis was quantified in the retrospective cohort (Fig. 2C). We confirmed that Olig2 was not expressed by astrocytes in control or WMI cases (Fig. 5A, B; Supplemental Fig. 4A, B). Olig2 localized to both pre-myelinating stages of the OL lineage (Supplemental Fig. 4C, D) and to mature OLs (Supplemental Figure 5). The majority of WMI cases (11 out of 17) lacked myelination within the lesions, as assessed by staining for myelin basic protein (MBP). Myelination was sparse in the remaining WMI cases (Supplemental Fig. 6A–C) within diffuse gliotic lesions (Supplemental Fig. 6D, E).

In the retrospective cohort, the density of Olig2-labeled nuclei in lesions was significantly elevated relative to controls (36—79; $p<0{\cdot}0001$, Table S·6). Peri-lesions were also significantly elevated relative to peri-controls (55—98; $p<0{\cdot}0001$). When analyzed on an individual basis relative to age and region-matched controls (Fig. 5C), in 12 out of 14 WMI cases Olig2 was significantly elevated in both lesions ($p<0{\cdot}003$, Table S·21) and peri-lesions ($p<0{\cdot}03$). Figure 5D shows that GFAP and Olig2 levels were significantly associated ($p<0{\cdot}005$, Table S·7). Hence, the total population of OL lineage cells was diffusely elevated rather than depleted in chronic lesions with diffuse astrogliosis.

To determine whether the increase in density of Olig2-labeled cells in WMI cases was due to a proliferative response, we quantified the density of cells that labeled with the cell cycle-proliferation marker Ki67. Ki67-labeled cells were detected in a subpopulation of both control and WMI cases (Supplemental Fig. 7A, B), but there was no significant difference in Ki67 density (Supplemental Fig. 7C) ($p=0{\cdot}69$, Table S·8). Since the density of Ki67-labeled cells was variable in both control and WMI cases, we considered whether this might be consistent with the activation of microglia during normal human white matter development or injury.[28] Nuclear staining for Ki67 was detected in Iba1-labeled cells (Supplemental Fig. 7D) and the density of Ki67 was significantly associated with the level of Iba1-labeled microglia (Supplemental Fig. 7E) ($p<0{\cdot}0001$; Table S·9). Given that early human WMI lesions sustain a significant depletion of preOLs,[13] the increased density of Olig2-labeled cells suggested that human OL lineage cells, as in rodents,[16] may undergo an early proliferative response that was not detectable in chronic lesions.

Expansion of the PreOL Pool and Failure of OL Maturation occurs in Chronic WMI Lesions

We employed the O4 and O1 antibodies to quantify preOLs (O4+O1−) relative to immature OLs (O4+O1+) in gliotic lesions defined by quantification of GFAP. PreOLs generate immature OLs, a population of pre-myelinating OLs that give rise to mature myelinating OLs. We analyzed contemporary cases (Table 2) where tissue processing was optimized to visualize pre-myelinating OL lineage stages.[12] Figure 6A, B shows the typical appearance of astrocytes, preOLs and immature OLs in control white matter. Chronic lesions had numerous reactive-appearing astrocytes and were enriched in preOLs (Fig. 6C, D) that were morphologically similar to controls. PreOL or OL degeneration was rarely seen in lesions with diffuse astrogliosis, which supported that delayed preOL death was not a prominent feature of WMI. Control and lesion white matter similarly contained infrequent apoptotic-appearing cells that displayed fragmented processes and condensed nuclei (Fig. 6E, F). Staining for caspase activation was also very low throughout white matter lesions in cases that survived for less than two weeks after birth (data not shown).

PreOL density was significantly elevated in WMI cases relative to controls (Fig. 7A) (28—67; p=0·0001, Table S·10). The density of immature OLs in WMI cases did not differ significantly from controls (Fig. 7B) (−1.2—7.5; p=0·14, Table S·11). The percentage of immature OLs was significantly reduced in WMI cases relative to controls (Fig. 7C) (−10·1—−3·5; p=0·0006, Table S·12). Pre-myelinating immature OLs were, thus, a minor population that did not show their normal developmental expansion. Hence, we addressed whether the magnitude of preOL expansion/arrest was related to the magnitude of astrogliosis. The density of preOLs was significantly associated with the level of GFAP (Fig. 7D) (p=0·0002, Table S·13). Thus, chronic WMI lesions displayed significant preOL maturation arrest as supported by accumulation of preOLs within gliotic lesions where the normal developmental increase in immature OLs also was not observed.

DISCUSSION

Neuroimaging studies support that advances in neonatal care have been accompanied by a pronounced reduction in the severity of WMI.[8] However, a recent retrospective study of archival cases from 1997–1999 proposed that a shift has occured from larger (macroscopic) necrotic lesions to microscopic necrotic foci observed with an incidence of 34%. These lesions appear to be largely undetected by MRI, but may cause myelination failure related to axonopathy.[9, 11] Consistent with this study, the incidence of microscopic necrosis in our contemporary cohort (2003–2010) was 36% in contrast to our retrospective cohort (1983–2000) where the incidence was 59%. However, in our contemporary cohort, the burden of microscopic necrosis was much lower than suggested by incidence data. Hence, the lower frequency of these lesions and their small size supports a significant reduction in the burden of necrosis and associated axonopathy compared to prior decades where much more axonopathy was observed.[10] Moreover, our data may reflect a more severe spectrum of WMI than occurs in preterm survivors, because it was derived from autopsy cases. The contribution of axonopathy to CP is likely to be variable and dependent on location of the lesions.

The declining burden of necrosis in contemporary cases supports that diffuse astrogliosis is the major pathological feature of WMI. Consistent with this conclusion, a prior retrospective study found that in cases with confirmed WMI, 82% had diffuse astrogliosis alone or in combination with microscopic necrosis.[9] Our data supports that WMI is currently accompanied by a significantly lower burden of microscopic necrosis, which is not detected by MRI. To better define the extent of diffuse astrogliosis and microscopic necrosis in preterm survivors, alternative approaches are needed to detect these lesions with higher resolution MRI. When high field strength MRI was applied in an experimental model of

preterm WMI, the sensitivity to detect diffuse astrogliosis approached 100% at 1 week after injury and microscopic necrosis was detected at sub-millimeter resolution with high sensitivity and specificity at two weeks.[31]

Human and experimental studies support a mechanism of myelination failure in perinatal WMI that involves a combination of degenerative, regenerative and arrested maturational processes that result in a net expansion in a pool of preOLs that fail to normally generate OLs. During the acute phase of WMI, if significant oxidative damage coincides with necrosis, both axonopathy and preOL loss were seen;[10, 14] whereas isolated preOL loss occurred when neuro-axonal degeneration was not associated with oxidative damage in fetal sheep or human.[13, 32] In contrast to chronic WMI in rodents,[16] where pronounced caspase-dependent preOL death was observed during the first 10 days after hypoxia-ischemia, minimal delayed caspase activation was observed by us, in cases with PVL,[3] or in WMI in fetal sheep within two weeks after ischemia.[31] We speculate that acute preOL death alone may be sufficient to trigger diffuse astrogliosis.

The pathophysiological significance of diffuse astrogliosis may be related to an aberrant regenerative response that involves preOL maturation-arrest. In the rat and fetal sheep, total preOL degeneration from acute and delayed mechanisms of death represented a small fraction of the total preOLs that were present during the chronic phase of WMI.[16, 31] In many of our human WMI cases, reduction in OL differentiation occurred during a developmental window when preterm white matter normally transitions to early myelination.[12, 33] However, we found that chronic astrogliotic lesions had an increased density of total OL lineage cells and preOLs that coincided with reduced OL differentiation. By contrast, no difference in Olig2-labeled cells was found in a study of chronic PVL lesions,[3] which averaged Olig2 counts from multiple cerebral regions without region-matching to controls. Region-matching is necessary, since the density of OL lineage cells varies markedly between regions.[13] Our studies from rodent, fetal sheep and human provide the first evidence that in diffuse WMI preOLs regenerate but survive in a state of arrested maturation that reduces the pool of OLs available for myelination.[16, 21, 31, 34]

The low level of delayed degeneration of preOLs and other glia within chronic WMI lesions has relevance for the direction of future studies to develop therapeutic interventions to prevent WMI. Given the robust intrinsic plasticity of preOLs to regenerate after WMI, our findings suggest that strategies directed at prevention of preOL death during the early phase of injury maybe a less viable strategy than to promote regeneration and repair during the delayed phase of injury. The therapeutic window to reverse preOL arrest is presently unclear.

That we were unable to identify a late proliferative OL lineage response in our cohorts of chronic WMI cases suggests that proliferation of OL progenitors may occur during an earlier phase of injury. In perinatal rodents, acute preOL degeneration from hypoxia-ischemia was followed by a rapid increase in preOL density within 24 hours that was related to proliferation of the OL progenitors that generate preOLs.[16, 21] Proliferation of the OL progenitor pool was not addressed in a prior study of chronic PVL, and no evidence for proliferation of other cell types was found.[3]

The mechanisms that mediate inhibition of OL maturation following CNS insults are largely unknown. Wnt transcriptional activation,[35] Notch signaling,[36] and bone morphogenetic protein[37] have been implicated in the inhibitory processes linked to OPC maturation arrest and remyelination failure. Arrest of preOL maturation is also stimulated both in vitro and in vivo by hyaluronan derived from reactive astrocytes.[15, 26, 38] Diffuse astrogliosis was significantly associated with reduced OL maturation, and robust expression of hyaluronan

and CD44 was detected in lesions, consistent with the injury response observed in demyelinating lesions, traumatic spinal cord injury, and ischemic lesions.[15, 39, 40] Although our study does not directly test the significance of elevated CD44 and HA in WMI lesions, adult mice lacking CD44 demonstrated a 50% reduction in ischemic infarcts following transient and long-term occlusion of the middle cerebral artery.[27] Transgenic overexpression of CD44 in the developing brain leads to dysmyelination and preOL accumulation.[41] Furthermore, during development, hyaluronan in the neural stem cell niche appears to hold progenitors in a quiescent state until differentiation is initiated.[42] Hence, disruption of hyaluronan-mediated inhibition of preOL differentiation is one of several potential strategies to promote myelination.

PreOL maturation-arrest appears to expand the developmental window of white matter immaturity, which may enhance the risk of recurrent and potentially more severe brain injury in critically ill premature infants. In rodents, the selective vulnerability of preOLs to hypoxia-ischemia not only persisted, but markedly increased with recurrent insult.[16] Additional serial neuro-imaging studies are needed to define the progression of WMI in preterm as well as term infants.[43, 44] Such studies are already defining clinical features that identify infants at risk for exacerbation of initial cerebral injury (e.g., preterm newborns with postnatal sepsis).[45]

Our results are consistent with growing evidence that neuroinflammatory mediators may exacerbate WMI, disrupt white matter maturation and contribute to repair.[46–48] Our quantitative analysis of astroglial responses to WMI unexpectedly found that the astroglial reaction was more extensive than previously defined by standard histopathological approaches. Astrocytes were diffusely more reactive both within lesions and the peri-lesion surround. This diffuse astroglial reaction appears to be part of a more generalized neuroinflammatory response that includes chronic microglial activation. The significant association of preOL arrest with the magnitude of astroglial activation suggests that this neuro-inflammatory environment may disrupt myelinogenesis via mechanisms directed at the preOL or at preOL-axonal interactions.

Future studies are needed in relevant experimental models and from human autopsy studies to define the evolution of myelination failure in chronic WMI. It is unknown whether myelination is delayed or permanently arrested after WMI. Such information is of critical importance to define the period over which the glial scar remodels and preOL arrest persists. Our studies underscore the need to further define the sensitivity and specificity of MRI to follow the evolution of diffuse WMI and myelination failure within chronic lesions. High-field MRI may provide a sensitive means to detect diffuse WMI[31] to evaluate potential thereapeutic strategies. These may include stem cell delivery or agents aimed at reversing preOL arrest to promote regeneration and repair of injured white matter in preterm survivors with cerebral palsy and cognitive impairment.

Supplementary Material

Refer to Web version on PubMed Central for supplementary material.

Acknowledgments

Supported by the NIH (National Institutes of Neurological Diseases and Stroke, 1RO1NS054044, and R37NS045737-06S1/06S2 (SAB) and 1F30NS066704 (AR)) a Bugher Award from the American Heart Association (SAB) and the March of Dimes Birth Defects Foundation (SAB). SPM is supported by a Canada Research Chair in Neonatal Neuroscience, a Michael Smith Foundation for Health Research Scholar award and a Canadian Institutes of Health Research Clinician Scientist award.

References

1. Volpe, JJ. Neurology of the Newborn. Philadelphia: W.B. Saunders; 2008.
2. Bax M, Tydeman C, Flodmark O. Clinical and MRI correlates of cerebral palsy: the European Cerebral Palsy Study. JAMA. 2006; 296(13):1602–1608. [PubMed: 17018805]
3. Billiards S, Haynes R, Folkerth R, NS B, Trachtenberg F, Rowitch D, et al. Myelin abnormalities without oligodendrocyte loss in periventricular leukomalacia. Brain Pathology. 2008; 18(2):153–163. [PubMed: 18177464]
4. Inder TE, Anderson NJ, Spencer C, Wells S, Volpe JJ. White matter injury in the premature infant: a comparison between serial cranial sonographic and MR findings at term. AJNR Am J Neuroradiol. 2003; 24(5):805–809. [PubMed: 12748075]
5. Counsell S, Allsop J, Harrison M, Larkman D, Kennea N, Kapellou O, et al. Diffusion-weighted imaging of the brain in preterm infants with focal and diffuse white matter abnormality. Pediatrics. 2003; 112(1):176–180. [PubMed: 12837883]
6. Chau V, Poskitt KJ, McFadden DE, Bowen-Roberts T, Synnes A, Brant R, et al. Effect of chorioamnionitis on brain development and injury in premature newborns. Ann Neurol. 2009; 66(2):155–164. [PubMed: 19743455]
7. Hamrick S, Miller SP, Leonard C, Glidden D, Goldstein R, Ramaswamy V, et al. Trends in severe brain injury and neurodevelopmental outcome in premature newborn infants: the role of cystic periventricular leukomalacia. J Pediatr. 2004; 145(5):593–599. [PubMed: 15520756]
8. Ment LR, Hirtz D, Huppi PS. Imaging biomarkers of outcome in the developing preterm brain. Lancet Neurol. 2009; 8(11):1042–1055. [PubMed: 19800293]
9. Pierson CR, Folkerth RD, Billiards SS, Trachtenberg FL, Drinkwater ME, Volpe JJ, et al. Gray matter injury associated with periventricular leukomalacia in the premature infant. Acta Neuropathol. 2007; 114(6):619–631. [PubMed: 17912538]
10. Haynes RL, Billiards SS, Borenstein NS, Volpe JJ, Kinney HC. Diffuse axonal injury in periventricular leukomalacia as determined by apoptotic marker fractin. Pediatr Res. 2008; 63(6): 656–661. [PubMed: 18520330]
11. Volpe JJ. Brain injury in premature infants: a complex amalgam of destructive and developmental disturbances. Lancet Neurology. 2009; 8:110–124. [PubMed: 19081519]
12. Back SA, Luo NL, Borenstein NS, Levine JM, Volpe JJ, Kinney HC. Late oligodendrocyte progenitors coincide with the developmental window of vulnerability for human perinatal white matter injury. J Neurosci. 2001; 21(4):1302–1312. [PubMed: 11160401]
13. Back SA, Luo NL, Mallinson RA, O'Malley JP, Wallen LD, Frei B, et al. Selective vulnerability of preterm white matter to oxidative damage defined by F_2-isoprostanes. Ann Neurol. 2005; 58:108–120. [PubMed: 15984031]
14. Haynes RL, Folkerth RD, Keefe RJ, Sung I, Swzeda LI, Rosenberg PA, et al. Nitrosative and oxidative injury to premyelinating oligodendrocytes in periventricular leukomalacia. J Neuropathol Exp Neurol. 2003; 62(5):441–450. [PubMed: 12769184]
15. Back S, Tuohy T, Chen H, Wallingford N, Craig A, Struve J, et al. Hyaluronan accumulates in demyelinated lesions and inhibits oligodendrocyte progenitor maturation. Nat Med. 2005; 9:966–972. [PubMed: 16086023]
16. Segovia K, Mcclure M, Moravec M, Luo N, Wang Y, Gong X, et al. Arrested oligodendrocyte lineage maturation in chronic perinatal white matter injury. Ann Neurol. 2008; 63(4):517–526.
17. Ballabh P, Xu H, Hu F, Braun A, Smith K, Rivera A, et al. Angiogenic inhibition reduces germinal matrix hemorrhage. Nat Med. 2007; 13(4):477–485. [PubMed: 17401377]
18. Mouton, P. Principles and practices of unbiased stereology: an introduction for bioscientists. Baltimore: Johns Hopkins University Press; 2002.
19. Wirenfeldt M, Clare R, Tung S, Bottini A, Mathern G, Vinters H. Increased activation of Iba1+ microglia in pediatric epilepsy patients with Rasmussen's encephalitis compared with cortical dysplasia and tuberous sclerosis complex. Neurobiol Dis. 2009; 34:432–440. [PubMed: 19285133]
20. Back S, Craig A, Luo N, Ren J, Akundi R, Rebeiro I, et al. Protective effects of caffeine on chronic hypoxia-induced perinatal white matter injury. Ann Neurol. 2006; 60(5):696–705. [PubMed: 17044013]

21. Back SA, Han BH, Luo NL, Chrichton CA, Tam J, Xanthoudakis S, et al. Selective vulnerability of late oligodendrocyte progenitors to hypoxia-ischemia. J Neurosci. 2002; 22(2):455–463. [PubMed: 11784790]
22. Back SA, Luo NL, Borenstein NS, Volpe JJ, Kinney HC. Arrested oligodendrocyte lineage progression during human cerebral white matter development: dissociation between the timing of progenitor differentiation and myelinogenesis. J Neuropathol Exp Neurol. 2002; 61(3):197–211. [PubMed: 11853021]
23. Kinney H, Back S. Human oligodendroglial development: relationship to periventricular leukomalacia. Semin Pediatr Neurol. 1998; 5(3):180–189. [PubMed: 9777676]
24. Friede, RL. Developmental Neuropathology. 2nd ed. Berlin: Springer-Verlag; 1989.
25. Hirayama A, Okoshi Y, Hachiya Y, Ozawa Y, Ito M, Kida Y, et al. Early immunohistochemical detection of axonal damage and glial activation in extremely immature brains with periventricular leukomalacia. Clin Neuropathol. 2001; 20(2):87–91. [PubMed: 11327303]
26. Sherman L, Back S. A GAG reflex prevents repair of the damaged CNS. Trends Neurosci. 2008; 31(1):44–52. [PubMed: 18063497]
27. Wang X, Xu L, Wang H, Zhan Y, Pure E, Feuerstein G. CD44 deficiency in mice protects brain from cerebral ischemia injury. Journal of Neurochemistry. 2002; 83(5):1172–1179. [PubMed: 12437588]
28. Billiards SS, Haynes RL, Folkerth RD, Trachtenberg FL, Liu LG, Volpe JJ, et al. Development of microglia in the cerebral white matter of the human fetus and infant. J Comp Neurol. 2006; 497(2): 199–208. [PubMed: 16705680]
29. Haynes RL, Folkerth RD, Trachtenberg FL, Volpe JJ, Kinney HC. Nitrosative stress and inducible nitric oxide synthase expression in periventricular leukomalacia. Acta Neuropathol. 2009; 118(3): 391–399. [PubMed: 19415311]
30. Arai Y, Deguchi K, Mizuguchi M, Takashima S. Expression of b-amyloid precursor protein in axons of periventricular leukomalacia brains. Pediatr Neurol. 1995; 13:161–163. [PubMed: 8534283]
31. Riddle A, Dean J, JR B, Gong X, Maire J, Chen K, et al. Histopathological correlates of MRI-defined chronic perinatal white matter injury. Ann Neurol. 2011 in press.
32. Riddle A, Maire J, Gong X, Chen K, CD K, AR H, et al. Differential susceptibility to axonopathy in necrotic and non-necrotic perinatal white matter injury. Stroke. 2011 under minor revision.
33. Jakovcevski I, Filipovic R, Mo Z, Rakic S, Zecevic N. Oligodendrocyte development and the onset of myelination in the human fetal brain. Front Neuroanat. 2009; 3:5. [PubMed: 19521542]
34. Zhiheng H, Liu J, Cheung P-Y, Chen C. Long-term cognitive impairment and myelination deficiency in a rat model of perinatal hypoxic-ischemia brain injury. Brain Res. 2009; 1301:100–109. [PubMed: 19747899]
35. Fancy S, Harrington E, Yuen T, Silbereis J, Zhao C, Baranzini S, et al. Axin2 as regulatory and therapeutic target in newborn brain injury and remyelination. Nature Neurosci. 2011 in press.
36. John G, Shankar S, Shafit-Zagardo B, Massimi A, Lee S, Raine C, et al. Multiple sclerosis: re-expression of a developmental pathway that restricts oligodendrocyte maturation. Nat Med. 2002; 8:1115–1121. [PubMed: 12357247]
37. Wang Y, Cheng X, He Q, Zheng Y, Kim D, Whittemore S, et al. Astrocytes from the contused spinal cord inhibit oligodendrocyte differentiation of adult oligodendrocyte precursor cells by increasing the expression of bone morphogenetic proteins. J Neurosci. 2011; 31:6053–6058. [PubMed: 21508230]
38. Sloane J, Batt C, Ma Y, Harris Z, Trapp B, Vartanian T. Hyaluronan blocks oligodendrocyte progenitor maturation and remyelination through TLR2. Proc Natl Acad Sci USA. 2010; 107(25): 11555–11560. [PubMed: 20534434]
39. Struve J, Maher P, Li Y, Kinnery S, Fehlings MG, Kuntz Ct, et al. Disruption of the hyaluronan-based extracellular matrix in spinal cord promotes astrocyte proliferation. GLIA. 2005; 52(1):16–24. [PubMed: 15892130]
40. Wang X, Zhan Y, Xu L, Feuerstein G, Wang X. Use of subtractive hybidization for differential gene expression in stroke: discovery of CD44 gene expression and localization in permanent focal stroke in rats. Stroke. 2001; 32(4):1020–1027. [PubMed: 11283406]

41. Tuohy T, Wallingford N, Liu Y, Chan F, Rizvi T, Xing R, et al. CD44 overexpression by oligodendrocytes: a novel mouse model of inflammation-independent demyelination and dysmyelination. GLIA. 2004; 47:335–345. [PubMed: 15293231]

42. Sherman, L.; Feistel, K. Glycoforum: Science of Hyaluronan. 2008. Hyaluronan as a regulatory component of neural stem cell and progenitor cell niches. Http://www.glycoforum.gr.jp/science/hyaluronan/HA30/HA30E.html.

43. Miller S, Ferriero D. From selective vulnerability to connectivity: insights from newborn brain imaging. Trends Neurosci. 2009; 32(9):496–505. [PubMed: 19712981]

44. Miller S, McQuillen P, Hamrick S, Xu D, Glidden D, Charlton N, et al. Abnormal brain development in newborns with congenital heart disease. N Engl J Med. 2007; 357(19):1971–1973. [PubMed: 17989392]

45. Glass HC, Bonifacio SL, Chau V, Glidden D, Poskitt K, Barkovich AJ, et al. Recurrent postnatal infections are associated with progressive white matter injury in premature infants. Pediatrics. 2008; 122(2):299–305. [PubMed: 18676547]

46. Czeh M, Gressens P, Kaindl AM. The Yin and Yang of Microglia. Dev Neurosci. 2011

47. Favrais G, van de Looij Y, Fleiss B, Ramanantsoa N, Bonnin P, Stoltenburg-Didinger G, et al. Systemic inflammation disrupts the developmental program of white matter. Ann Neurol. 2011 in press.

48. Dean J, van de Looij Y, Sizonenko S, Lodygensky G, Lazeyras F, Bolouri H, et al. Delayed Cortical Impairment Following Lipopolysaccharide Exposure in Preterm Fetal Sheep. Ann Neurol. 2011 in press.

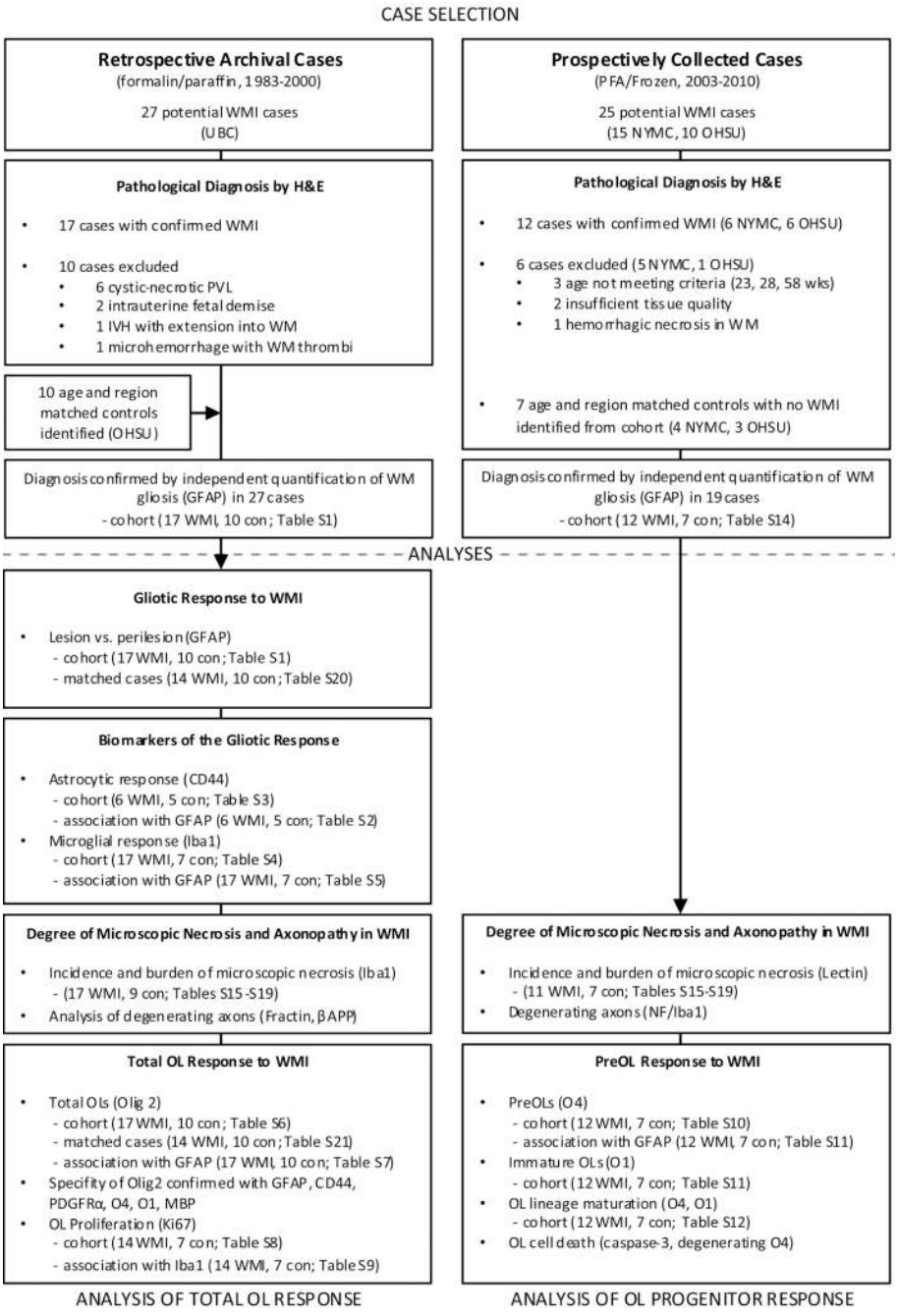

Figure 1.

Schematic Diagram showing the design of the study and the statistical tests applied to the different arms of the study (indicated by references to the statistical subtables, see Supplemental Table 1). Abbreviations: GMH, germinal matric hemorrhage; H & E, hematoxylin and eosin; IVH, intraventricular hemorrhage; NYMC, New York Medical College; OHSU, Oregon Health & Science University; OL, oligodendrocyte; PFA, paraformaldehyde; UBC, University of British Columbia; WMI, white matter injury

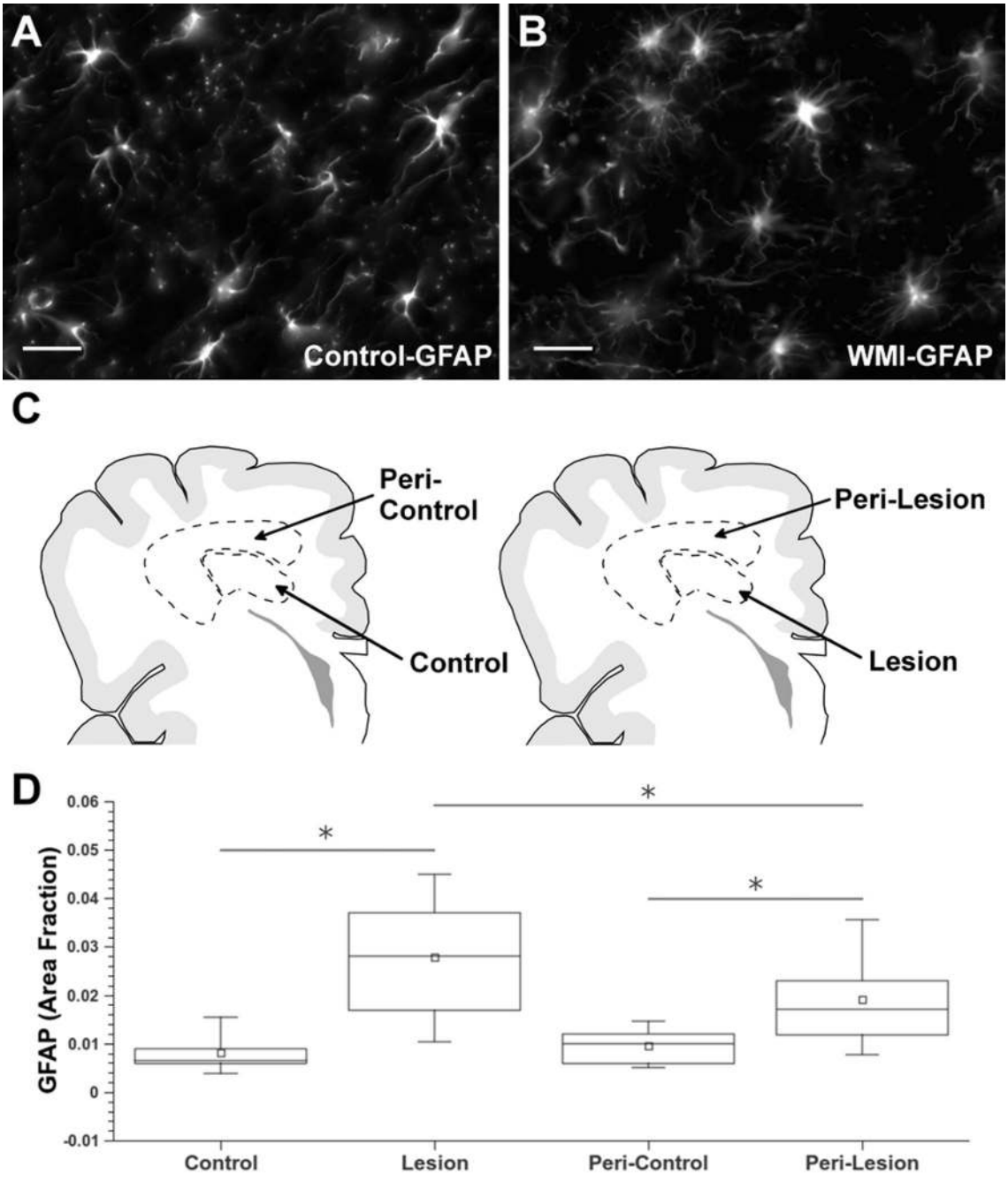

Figure 2.

Diffuse astroglial reaction in chronic WMI defined by astrocyte quantification. (A, B) Typical morphology of GFAP-labeled astrocytes in white matter from control (A) and WMI (B) cases at 29 weeks PCA selected from the retrospective cohort (Table 1). (C) Schematic representation of the regions of interest (ROIs) selected for astrocyte quantification. The ROIs for control cases (control/peri-control; left) were age- and region-matched to corresponding ROIs for WMI cases (lesion/peri-lesion; right). (D) Astroglial quantification identified significant graded astroglial reaction in lesion and peri-lesion ROIs that was also significantly elevated relative to control and peri-control ROIs, respectively (*p<0·0001). Scale bars: 25 μm.

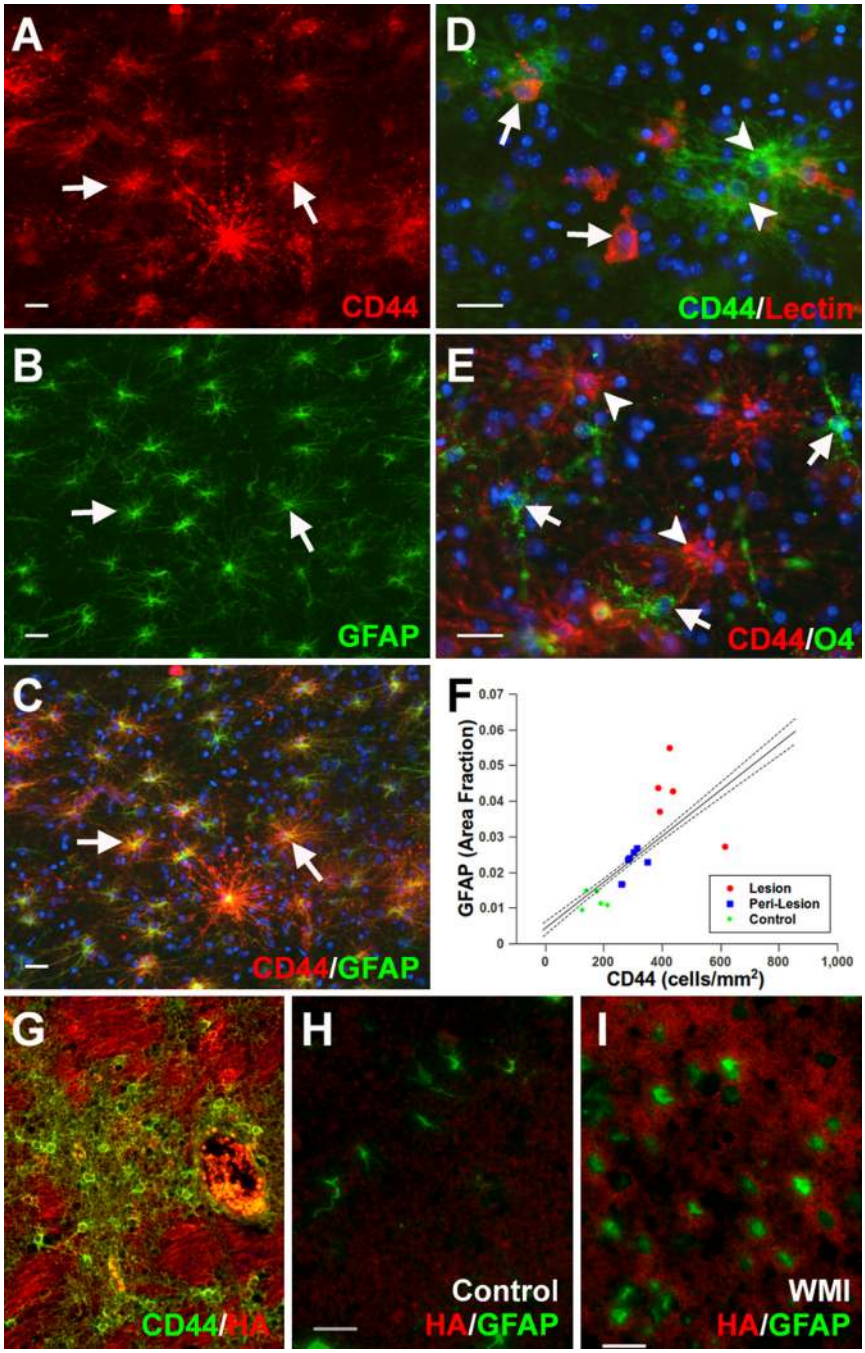

Figure 3.

The hyaluronan (HA) receptor CD44 is an independent marker of gliosis that is upregulated in HA-rich chronic WMI lesions. (A–C) CD44 (A) is highly expressed on the majority of GFAP-labeled astrocytes (B; arrows indicate typical double-labeling); merge in C. (D) CD44 staining localized to astrocytes (green; arrowhead) but not to microglia/macrophages labeled with tomato lectin (arrows; red). (E) CD44 staining was specific to astrocytes (red; arrowhead) but did not localize to O4 antibody-labeled oligodendrocyte progenitors (arrows; green). (F) CD44 and GFAP were significantly associated ($p<0{\cdot}0001$) when analyzed across the entire retrospective cohort of control and WMI cases (Table 1). Dashed lines are the 95% confidence intervals. Each graphical data point represents the mean for each subject

and is presented for visual clarity. See Table S·2 for statistical analysis. (G) A representative case of chronic WMI where pericellular HA (red) was highly enriched in the extracellular matrix in close association with CD44-labeled reactive astrocytes (green). (H, I) HA (red) and GFAP levels (green) were low in controls (H) relative to WMI cases (I) where the diffuse pericellular HA (red) surrounds GFAP-labeled astrocytes (green). Scale bars: 25 μm.

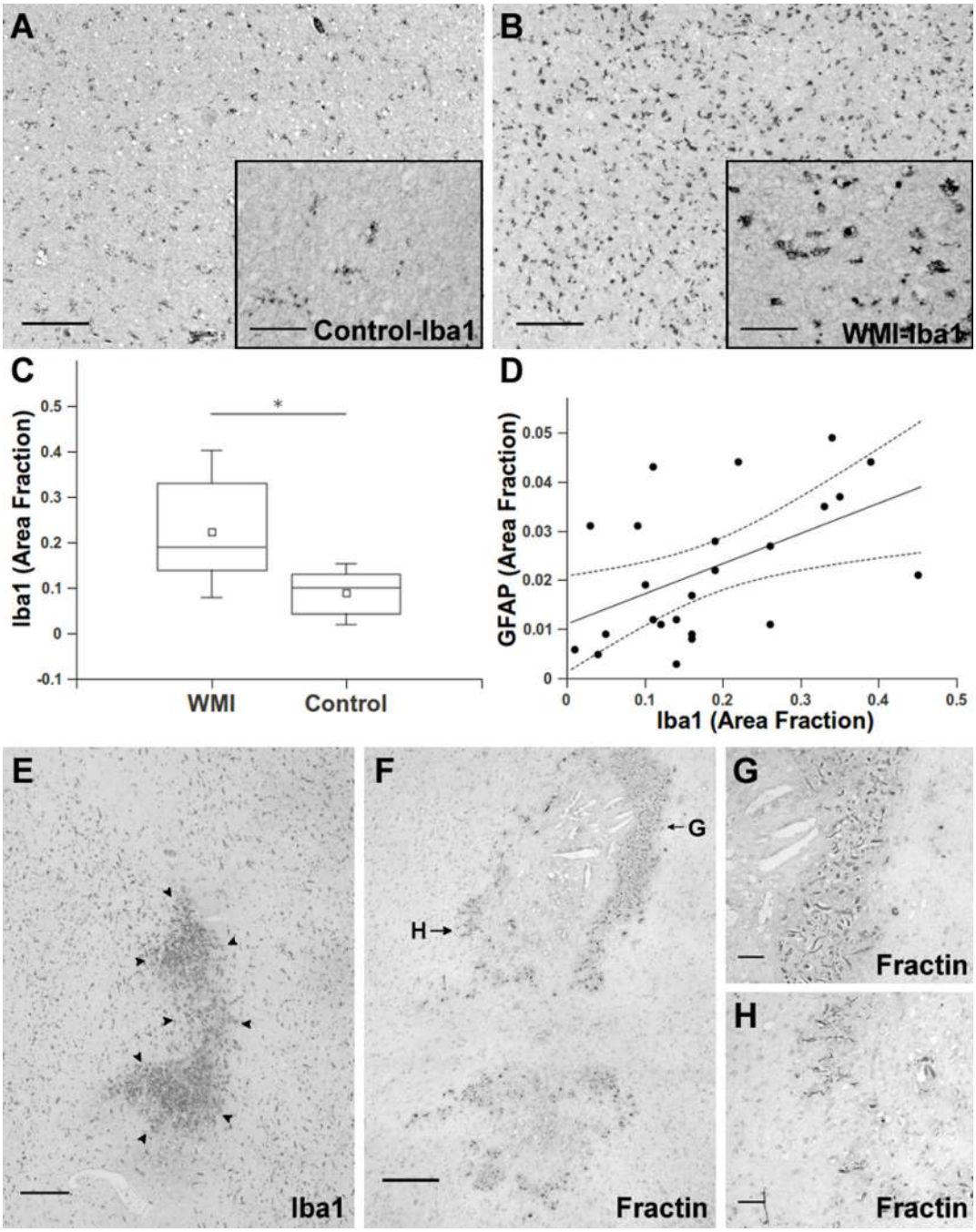

Figure 4.

Microglia activation persists in chronic WMI lesions and identifies microcysts that coincide with focal axonopathy. (A, B) Typical appearance of resting microglia stained for Iba1 in controls (A) and ramified/ activated microglia in WMI lesions (B) from cases at 38 weeks PCA. Insets show higher power detail of the cells in A and B. (C) The total area of Iba1-labeled cells was significantly elevated (*p=0·01) in the retrospective WMI cases (Table 1) relative to controls. (D) Iba1 and GFAP were significantly associated (p=0·002) when analyzed across the entire cohort of control and WMI cases. Dashed lines are the 95% confidence intervals for the group analysis. (E) Typical appearance of a microscopic focus of necrosis (microcyst) in the periventricular white matter, which was first identified by H &

E staining and confirmed by Iba1 staining of microglia/macrophages (arrowheads). (F) Axonal degeneration was restricted to microcysts as visualized with the Fractin antibody. Fractin staining was mainly localized to the periphery of the necrotic foci. (G, H) High power details of the degenerating axons in panel F show numerous swollen and dystrophic-appearing axons.
Scale bars: A, B, E, F, 250 μm; A and B insets, G, H, 50 μm.

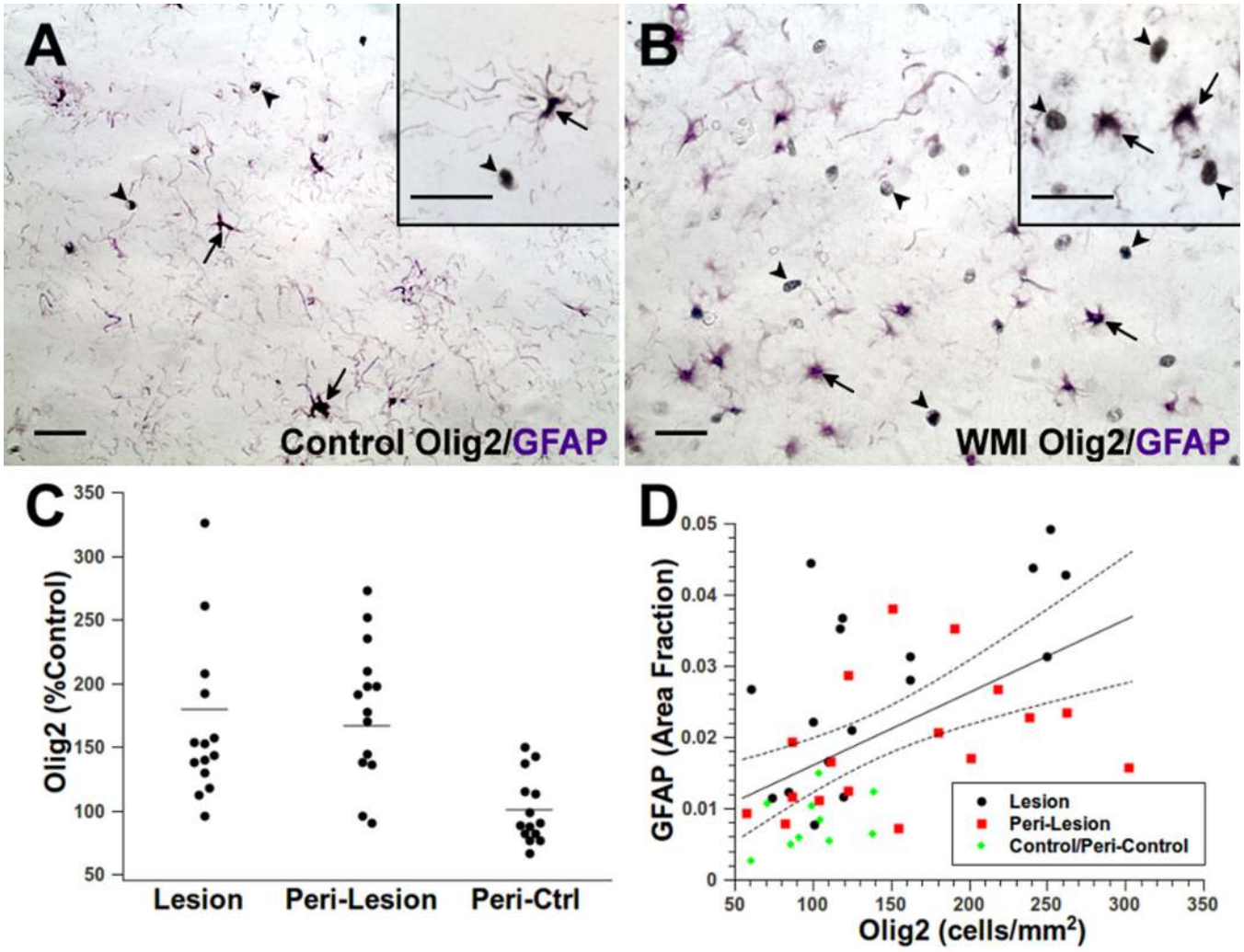

Figure 5.

The total population of oligodendrocyte lineage cells is increased in WMI. (A, B) Typical distribution of Olig2-labeled nuclei (black; arrowheads) and GFAP-labeled astrocytes (purple; arrows) in controls (A) and WMI cases (B). Insets provide higher power detail of the difference in morphology between Olig2 and GFAP staining. See also Supplemental Fig. 5A. (C) Olig2-labeled nuclei were significantly elevated in WMI cases (lesion and peri-lesion) relative to control (see text and Table S·21 for results of statistical analysis). (D) Olig2 and GFAP were significantly associated ($p<0{\cdot}005$) when analyzed across the retrospective cohort of control and WMI cases (Table 1). Dashed lines are the 95% confidence intervals for the group analysis. Scale bars: A, B and insets for A, B, 25 μm.

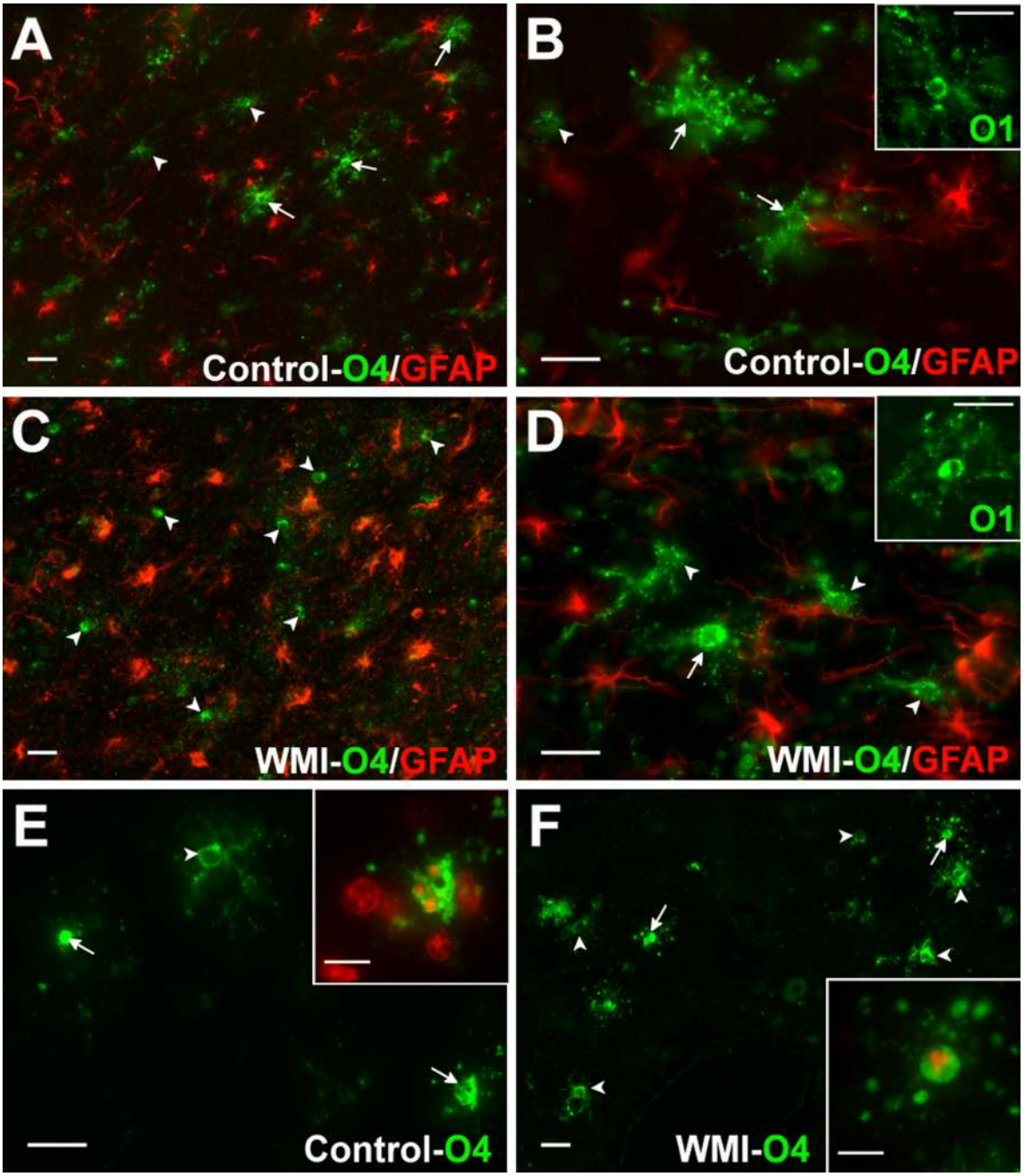

Figure 6.

Responses of pre-myelinating OL lineage stages in chronic WMI lesions.

(A, B) Typical morphology and distribution of O4-labeled preOLs (arrowheads) and immature OLs (arrows) in control white matter from a case at 29 weeks PCA. Note the paucity of reactive-appearing GFAP-labeled astrocytes (red). Immature OLs (green; arrows and inset: O1-labeled cell) were frequently visualized. (C, D) WMI lesion (34 weeks PCA) showing numerous reactive-appearing astrocytes (red) and an increased number of O4-labeled preOLs (green; arrowheads) relative to immature OLs (green; arrows and inset: O1-labeled cell). (E, F) Typical morphology of degenerating O4-labeled cells (arrows) that were rarely seen in controls (E) or WMI lesions (F) from cases at 29 weeks PCA. Such cells were

morphologically distinct from intact cells (arrowheads). Inset in E (control) shows a detail of cell at lower right (arrow) with typical nuclear fragmentation of a degenerating cell surrounded by normal-appearing nuclei visualized by Hoechst (red). Inset in F (WMI) shows higher power detail of the degenerating cell at upper right (arrow); note condensed nucleus and fragmented processes of the degenerating cell. Scale bars: A–F, 25 μm; insets for E, F, 10 μm.

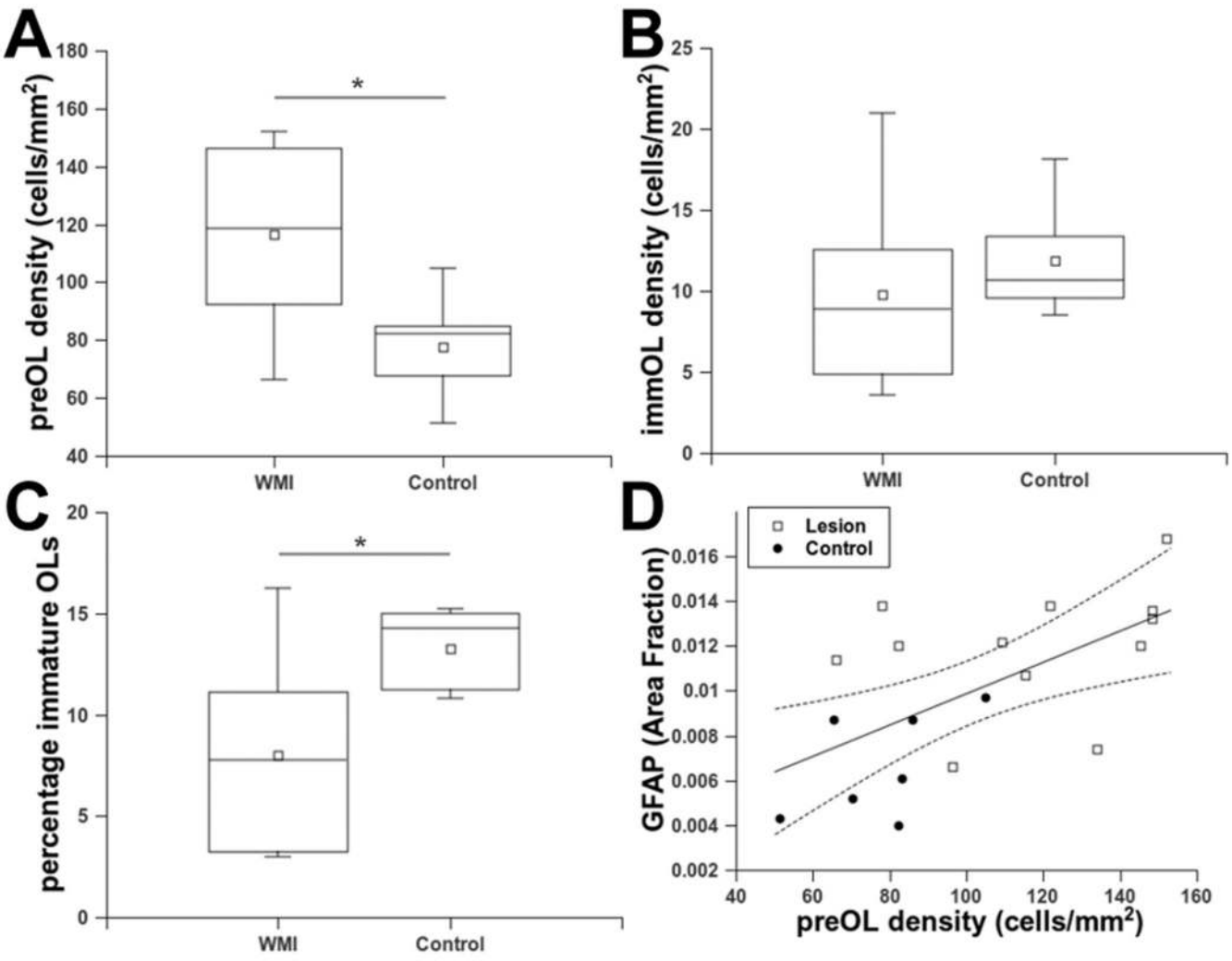

Figure 7.

Expansion of the preOL pool coincides with failure of OL maturation in WMI.

(A) An analysis of preOL density from the prospectivelly collected cases (table 2) found a significant elevation in WMI lesions relative to controls (*p<0·0001). (B) Analysis of the same cohort as in A found no significant difference in OL density in WMI cases vs. controls (p=0·14). (C) The percentage of OLs was significantly reduced in WMI cases vs. controls (*p=0·0006). (D) PreOL density and GFAP were significantly associated (p=0·002) when analyzed across the entire cohort of control and WMI cases. Dashed lines are the 95% confidence intervals for the group analysis.

Table 1

Summary of Clinical and Neuropathological Data for 24 Cases Studied from Paraffin-Embedded Archival Tissue

Case	Primary Diagnosis	PCA	ST	PMI	Sex	Clinical Diagnosis, Cause of Death	Other Neuropathological Diagnosis
1	WMI	32	<1	24	M	HF-NI of uncertain etiology, pulmonary hypoplasia	None
2	WMI	32	1	24	F	Meningitis and ventriculitis (*E. coli*), DIC	Meningitis and ventriculitis, germinal matrix hemorrhage, cerebellar hemorrhage
3	WMI	32	3	24	F	IUGR, neonatal adenovirus infection with necrotizing bronchitis	PV infarcts, hippocampal and subicular necrosis
4	WMI	32	6	48	M	BPD, sepsis, renal failure	None
5	WMI	34	<1	72	M	VATER complex, hypoventilation secondary to airway obstruction	Cerebellar heterotopia
6	WMI	34	2	72	M	Acute severe chorioamnionitis and funisitis, RDS, pneumonia	Neuronal loss in thalamus, brainstem, and hippocampus
7	WMI	34	2	24	M	HMD/RDS, sepsis, recurrent cardiac decompensation	Neuronal loss and gliosis in thalamus, kernicterus in subthalamic body, floor of 4th ventricle, and pontomedullary junction, hemorrhage of choroid plexus, necrosis of anterior horn of spinal cord
8	WMI	37	1	72	F	HMD/RDS, pneumonia,	None
9	WMI	37	2	48	M	HMD/RDS, unilateral left lung agenesis, necrotizing tracheobronchitis	Ventricular enlargement, resorbing germinal matrix hemorrhage, choroids plexus hemorrhage
10	WMI	38	<1	24	M	Meconial aspiration, gastroschisis	Neuronal loss in basis pontis
11	WMI	38	1	48	M	Transposition of great arteries, perioperative complications	None
12	WMI	38	9	24	M	Beckwith-Weideman syndrome, BPD, pneumonia	Subcortical heterotopias, hydromyelia in spinal cord
13	WMI	38	13	24	F	HMD/RDS, BPD, NEC with candida peritonitis	Partial agenesis of CC, old IVH
14	WMI	40	<1	24	M	Hypoplastic left heart syndrome with severe aortic valve stenosis, hypoplasia of left ventricle and atrium, congestive heart failure	None
15	WMI	41	2	24	M	Pulmonary valve atresia with tricuspid incompetence, PDA, congestive heart failure	Cortical gliosis and neuronal loss
16	WMI	43	18	24	M	BPD, recurrent NEC, sepsis (*Enterobacter*), myocardial ischemia, renal failure	Neuronal injury and neuro-axonal swelling in pons, lateral geniculate body, hippocampus, cerebral cortex with dilated ventricles
17	WMI	48	22	48	F	HF-NI secondary to in utero WPW and heart failure, maternal mirror syndrome	None
18	Control	31	<1	72	M	Bladder outlet obstruction, imperforate anus, diaphragmatic hernia	None
19	Control	33	$1^{5/7}$	20	F	Monozygotic twin, IUGR, renal hypoplasia	Mild hippocampal neuronal injury
20	Control	$33^{2/7}$	<1	20	M	Tracheal agenesis, esophageal stenosis, interrupted aorta	Mild subarachnoid hemorrhage
21	Control	35	<1	36	M	HF-NI	None
22	Control	$36^{3/7}$	<1	21	M	Bladder outlet obstruction, pulmonary hypoplasia	Mild WM gliosis, cerebellar heterotopias
23	Control	38	<1	12	M	HMD/RDS	Mild hippocampal neuronal injury

Case	Primary Diagnosis	PCA	ST	PMI	Sex	Clinical Diagnosis, Cause of Death	Other Neuropathological Diagnosis
24	Control	49	$15^{2/7}$	36	F	Tetralogy of Fallot, IUGR	Early cerebral edema

Data includes postconceptional age (PCA) in weeks at time of death (derived from gestational age at birth and survival time (ST) in weeks after birth), estimated post-mortem interval (PMI) in hours before tissue collection at autopsy and clinical data pertinent to the primary diagnosis.

BPD = bronchopulmonary dysplasia; CC = corpus callosum; DIC = disseminated intravascular coagulation; GMH = germinal matrix hemorrhage; HF-NI = hydropsfetalis, nonimmune; HMD/RDS = hyaline membrane disease/respiratory distress syndrome; IUGR = intrauterine growth retardation; IVH = intraventricularhemorrhage; NEC = necrotizing enterocolitis; PDA = patent ductusarteriosius; PV = periventricular; RDS = respiratory distress syndrome; VATER complex = Vertebral anomalies, anal atresia, tracheo-esophageal fistula, radial dysplasia, and cardiac anomalies; VSD = ventricular septal defect; WM = white matter; WMI = white matter injury; WPW = Wolf-Parkinson-White.

Table 2

Summary of Clinical and Neuropathological Data for 19 Prospectively Collected Cases

Case	Primary Diagnosis	PCA	ST	PMI	Sex	Clinical Diagnosis, Cause of Death	Other Neuropathological Diagnosis
1	WMI	29	<1	40	M	HF-NI, Hypoplastic right heart	None
2	WMI	$29^{2/7}$	$2^{2/7}$	12	M	Biventricular cardiac hypertrophy	GMH, mild neuronal injury in hippocampus and deep cerebellar nuclei
3	WMI	31	<1	12	M	HF-NI, respiratory failure	None
4	WMI	32	4	18	M	Pulmonary atresia, cardiac arrest	Subicular neuronal injury
5	WMI	33	<1	12	M	VSD, multi-cystic kidney, NEC, sepsis	None
6	WMI	33	$8^{4/7}$	20	M	Post-hemorrhagic hydrocephalus, pneumonia	GMH, grade IV IVH, neuronal loss/gliosis in hippocampus
7	WMI	$33^{1/2}$	<1	18	F	Diaphragmatic hernia, respiratory failure	Grade 2 IVH
8	WMI	34	$^{6/7}$	49	M	Polycythemia, recipient twin-twin transfusion syndrome, pericardial effusion	None
9	WMI	34	9	40	M	Peritonitis, cholestasis	Large rightchronic hemispheric hemorrhagic infarct, bilateral cerebellar infarcts, diffuse hippocampal and brainstem neuron loss
10	WMI	37	1	18	M	Diaphragmatic hernia, respiratory failure	None
11	WMI	$40^{1/2}$	<1	20	M	Hypoplastic right heart, cardio-respiratory failure	None
12	WMI	45	3	18	F	Aortic coarctation, VSD	Hippocampal neuronal injury
13	Control	$28^{5/7}$	$4^{1/7}$	26	M	NEC	Small focal GMH
14	Control	29	4	14	M	NEC, intestinal perforation, sepsis	Small GMH
15	Control	29	4	16	F	Endocarditis	Grade 2 IVH
16	Control	$29^{4/7}$	2	22	M	Oligohydramnios, IUGR	GMH with intraventricular extension
17	Control	31	1	12	M	Perforated ileum, respiratory failure	None
18	Control	33	$1^{5/7}$	20	F	Monozygotic twin, IUGR, renal hypoplasia	Mild hippocampalneuronal injury
19	Control	37	2	21	F	Diaphragmatic hernia and hypoplastic lung	None